Measurements of ground-state OH rotational energy-transfer rates

Dahv A. V. Kliner and Roger L. Farrow

Citation: The Journal of Chemical Physics **110**, 412 (1999); doi: 10.1063/1.478073
View online: http://dx.doi.org/10.1063/1.478073
View Table of Contents: http://scitation.aip.org/content/aip/journal/jcp/110/1?ver=pdfcov
Published by the AIP Publishing

Measurements of ground-state OH rotational energy-transfer rates

Dahv A. V. Kliner and Roger L. Farrow
Sandia National Laboratories, Combustion Research Facility, Livermore, California 94551

(Received 27 July 1998; accepted 25 September 1998)

We have studied rotational energy transfer (RET) in collisions of OH with the bath gases Ar, N_2, O_2, and H_2O at 293 K. Rotationally hot OH($X\ ^2\Pi_{3/2}$, $v''=0$, $N''=1-12$) was generated by photolysis of H_2O_2 at 266 nm, and collisional relaxation of the nascent rotational distribution was monitored by laser-induced fluorescence. The data are remarkably well described by an exponential-gap model for the matrix of state-to-state RET rate constants. For Ar, N_2, and O_2, RET rates are significantly faster at low N'' than high N''; for H_2O, RET is approximately an order of magnitude faster than for the other bath gases, and the rate is not as strongly dependent on N''. The rates of rotationally inelastic energy transfer are similar in the X and A states, but the X-state depopulation rate constants (including nearly elastic, Λ-doublet-changing collisions) are faster than the A-state values. By comparing the depopulation rates derived from the present experiment with previous linewidth measurements, we conclude that RET is the dominant source of pressure broadening for OH microwave transitions and makes a significant contribution for ultraviolet $A-X$ transitions. While generally good agreement is found between the present results and previous OH RET studies for both the ground and excited electronic states, some significant discrepancies are noted. © *1999 American Institute of Physics.* [S0021-9606(99)01701-8]

I. INTRODUCTION

Collisional processes profoundly influence the spectral properties of molecules.[1] Rotational energy transfer (RET) is particularly important for determining molecular line shapes and saturation behavior. Accurate knowledge of RET rates is thus essential for quantitative application of spectroscopic diagnostic methods such as absorption spectroscopy and laser-induced fluorescence (LIF),[2] and a large number of experimental and theoretical studies of RET have been reported.[3] Most experimental studies have been performed using stable molecules and/or molecules prepared in an electronically excited state. Relatively few RET measurements have been reported for transient species in the ground state. In this paper, we report measurements of RET rates of OH in the ground electronic and vibrational states ($X\ ^2\Pi_{3/2}$, $v''=0$) for collisions with Ar, N_2, O_2, and H_2O.

LIF detection of OH is widely used in a variety of applications, including laboratory studies, combustion measurements, and atmospheric sensing. For applications in which the temperature and/or composition are variable, e.g., combustion studies, knowledge of OH RET rates under the relevant conditions is required for accurate determination of OH densities and for OH thermometry.[4,5] Several studies of RET in electronically excited OH $A\ ^2\Sigma^+$ have been reported, including measurements of both state-to-state transfer rates and total depopulation rates (i.e., the sum of the state-to-state rates out of a given level); this work has been reviewed by Dagdigian[6] and by Kohse-Höinghaus.[2]

Fewer measurements of RET rates for ground-state OH $X\ ^2\Pi_{3/2}$ have been reported. Gericke and Comes[7] used the reaction of O(^1D) with H_2O to generate rotationally and vibrationally excited OH in the presence of excess H_2O; absorption spectroscopy was used to follow the time evolution of the OH rotational distribution in $v''=0-2$. Rotational relaxation of the OH was found to occur at a gas-kinetic rate, which was attributed to formation of a hydrogen-bonded $OH\cdot H_2O$ collision complex, and an average rate constant for rotational relaxation was obtained. Holtzclaw *et al.*[8] generated rotationally and vibrationally hot OH via the reaction of O(^1D) with H_2 and observed collisional relaxation of the rotational distribution by O_2 at 100 K for $v''=1-3$. The data were well described by a model in which $\Delta N''$ was restricted to be ± 1, with this assumption, state-to-state RET rate constants for $N''=8-25$ were determined, and a local minimum (''bottleneck'') was found at $N''=14$.

In related work, Andresen *et al.*[9] measured the total depopulation rate and the Λ-doublet-changing collision rate for OH($v''=1$, $J''=1.5,4.5$) in H_2. Copeland and Crosley[10] observed a propensity for Λ-doublet conservation in inelastic ($J''=1.5\rightarrow 2.5$) collisions of OH($v''=2$) with H_2O, and Wysong *et al.*[11] observed a propensity for conservation of total parity (not of Λ-doublet state) in spin-orbit-changing collisions of OH($v''=2$, $J''=2.5$) with He. Detailed crossed-molecular-beam studies of ground-state OH RET have also been reported.[9,12–14]

In the present experiment, rotationally hot OH($X\ ^2\Pi_{3/2}$, $v''=0$, $N''=1-12$) was generated by photolysis of H_2O_2 at 266 nm. Collisional relaxation of the OH by the bath gas (Ar, N_2, O_2, or H_2O) was monitored by recording LIF spectra at various times following photolysis. We find that RET by H_2O is approximately an order of magnitude faster than for the other colliders. Moreover, for Ar, N_2, and O_2, the OH rotational distribution at intermediate times is ''kinked,'' indicating more efficient RET for low N'' than high N''; in contrast, H_2O does not exhibit such a pronounced variation of RET rate with N''. To extract RET rate constants from the observed time evolution of the OH rota-

tional distribution, the data were fit using various models for the state-to-state RET rate matrix. An exponential-gap model is remarkably successful in reproducing the measured distributions for all four bath gases. We compare the derived state-to-state and depopulation rate constants with previous measurements of OH RET rates for both the ground and excited electronic states and with OH pressure-broadening studies. While generally good agreement is found, some significant discrepancies are noted.

II. EXPERIMENT

A. Overview

Photolysis of H_2O_2 at 266 nm produced rotationally hot $OH(v''=0)$ in a flow cell in the presence of excess bath gas (Ar, N_2, O_2, or H_2O), which collisionally relaxed the OH. The time evolution of the OH rotational population distribution was monitored by laser-induced fluorescence (LIF) using a variably delayed probe laser (~282 nm). The main components of the apparatus were: (i) the photolysis laser, (ii) the probe laser, (iii) the H_2O_2 source and flow cell, and (iv) the LIF collection and detection system. Each component and other experimental details are presented below.

B. Laser systems

The photolysis laser produced 266-nm pulses of 100-ps duration and 30 mJ of energy at a repetition rate of 20 Hz. In this system, selected pulses from a diode-pumped, mode-locked Nd:YAG laser (Lightwave Model 131, 100-ps pulse duration) were amplified in a Nd:YAG regenerative amplifier followed by two single-pass Nd:YAG amplification stages (Positive Light). The output of the final amplifier stage, consisting of 200-mJ pulses at 1064 nm, was frequency quadrupled using KD*P crystals. The 266-nm pulse energy was reduced to ~1 mJ incident at the photolysis cell using two beam splitters followed by a half-wave plate and MgF_2 Rochon polarizer (Halbo Optics). The photolysis beam was split into two beams of approximately equal intensity, which were crossed at a small angle in the flow cell. This geometry was a remnant of previous four-wave mixing experiments and was not required for the present study; it was advantageous, however, for reducing optical damage to the cell windows.

The probe laser produced tunable ~282-nm pulses of ~90-ps duration and 0.5 mJ of energy at a repetition rate of 20 Hz. A Nd:YAG laser (Coherent Infinity) pumped a distributed-feedback dye laser (DFDL), tunable from ~562 to 565 nm. The DFDL produced nearly transform-limited pulses of ~90-ps duration and 0.15-cm^{-1} linewidth, which were frequency doubled in an angle-tuned BBO crystal (Inrad Autotracker II). The probe laser was attenuated to ~50 μJ using a half-wave plate and polarizer to avoid saturation of the LIF transitions (see below). This arrangement also allowed the relative polarizations of the photolysis and probe lasers to be varied; in most experiments, these polarizations were parallel.

The probe laser was scanned from 281.2 to 282.1 nm, allowing detection of $N''=1-12$ (Sec. II F). Because of the large line spacings at high N'', the laser was not scanned continuously over this spectral region: slow scans were performed over the regions of interest, and the laser was scanned quickly between these regions. The wavelength of the DFDL was measured with a wavemeter (New Focus Model 7711, 0.001-nm resolution) and recorded at each point in a spectral scan; transmission of the DFDL output through an etalon (1.0-cm^{-1} free-spectral range) was also recorded to linearize the scan (i.e., to interpolate between wavemeter readings).

Each laser beam was collimated to a diameter of ~4 mm prior to entering the flow cell. The copropagating beams were crossed near the center of the cell, providing a several-cm-long overlap region. The delay between the photolysis and probe pulses was electronically variable over a wide range (>20 μs) with a jitter of at most ± 1 ns. The pulse energies of the two lasers were monitored with pyroelectric detectors (Molectron J3).

C. H_2O_2 source and flow cell

Hydrogen peroxide was obtained by flowing the bath gas through a bubbler (10–20-μm pore size) containing 50 wt. % aqueous H_2O_2 (Aldrich). The flow rate of the bath gas was 1–5 standard $cm^3\,s^{-1}$. The concentration of the H_2O_2 solution was verified prior to and following the experiments by measuring its density and its absorption spectrum in the 300–400-nm region. Comparison with literature values[15,16] indicated a composition of 48 ± 1 wt. % at the beginning of these experiments and 55 ± 1 wt. % at the end (i.e., the H_2O_2 solution had partially distilled during the course of the experiments). For the experiments with Ar, N_2, and O_2, the bubbler pressure was maintained at ~750 Torr, corresponding to a gas-phase composition of 99% bath gas, 0.82% H_2O, and 0.069% H_2O_2 (the vapor pressure of 50 wt. % H_2O_2 at 20 °C is 6.68 Torr, with 92.3% H_2O).[15] For experiments with H_2O as the bath gas, the boil-off from the bubbler was used directly (i.e., no additional flow was provided). The flow from the bubbler passed through a Teflon metering valve and a short length of PFA tubing before entering the cell.

The flow cell was a Pyrex cross with fused-silica windows terminating each arm. The laser beams propagated along the long axis of the cell, and the LIF was collected along one of the perpendicular arms. The cell could be evacuated to ~25 mTorr. For the present experiments, the cell pressure was regulated using a needle valve on the output port to within ± 0.1 Torr (± 0.05 Torr for a single scan) at ~1–8 Torr (depending on the bath gas). The pressures in the bubbler and flow cell were measured with capacitance manometers (MKS Baratron). The residence time in the ~300-cm^3 cell was typically ~30 s.

D. LIF collection and detection system

The LIF emitted perpendicular to the propagation axis of the laser beams was collected with an f/2 lens and focused with an f/4 lens onto the entrance slit of a 0.25-m monochromator (Oriel). A wide monochromator bandpass [~20 nm full width at half maximum (FWHM)] was used to allow collection of fluorescence originating from both $v'=0$ and $v'=1$. The spectrally filtered fluorescence was attenuated

with neutral density filters, as needed, before detection by a photomultiplier tube (PMT, Hamamatsu R955). The PMT pulses were amplified with a charge-integrating amplifier (EG&G Model 142), whose output was digitized using a 12-bit A/D converter. Similar A/D converters digitized the outputs of the pyroelectric detectors and of the photodiode that monitored the etalon transmission.

The digitized signals were recorded with a computer, which also controlled and recorded the DFDL wavelength. The LIF signal was normalized by the photolysis-and probe-laser energies on each shot before being averaged. Typically 20 shots were averaged at each wavelength, with a DFDL step size of 9×10^{-4} nm (corresponding to 0.05 cm^{-1} in the UV).

E. H_2O_2 photolysis and the initial OH rotational distribution

Gericke *et al.*[17] studied in detail the scalar and vector properties of the OH produced by 266-nm photolysis of H_2O_2. In this process, 10% of the 20 700 cm^{-1} of available energy is partitioned into OH rotation and 90% is partitioned into relative translation of the fragments ($<0.2\%$ appears as OH vibrational energy); the nascent OH is well characterized by a rotational temperature of 1530 ± 150 K. The OH spin-orbit states are statistically populated, and there is a small preference for the $\Pi(A'')$ (or f) Λ doublet.[18] The photodissociation process is rapid (i.e., instantaneous on the time scale of the present experiment): the lifetime of the electronically excited H_2O_2 is <60 fs.[17]

Translational relaxation of the nascent OH occurred more rapidly than rotational relaxation, as evidenced by the temporal evolution of the LIF line shapes (see Sec. II F). Moreover, for the bath gases Ar, N_2, and O_2, the OH rotational distribution measured at the earliest time (i.e., the smallest pressure-time product) was in good agreement with the expected nascent distribution[17] (Sec. III A). Thus, for these bath gases, translational relaxation of the nascent OH allowed RET to be monitored without the complication of distorted (broadened) line shapes and, more importantly, ensured that the measured RET rates correspond to thermally equilibrated collisions. For H_2O, RET was faster, and some rotational relaxation had occurred even at the earliest time. This result is in accord with a previous measurement[7] of the rate constant for OH translational relaxation by H_2O at 300 K of $>2.3\times10^{-10}$ $cm^3\,mol^{-1}\,s^{-1}$, corresponding to a relaxation time of <130 ns at 1 Torr. The H_2O RET data in the present experiment may therefore have a contribution from superthermal collisions, particularly at the earliest times.

The rate constant for Λ-doublet-changing collisions is comparable to that for translational relaxation;[9,10] the Λ-doublet states were therefore thermally equilibrated under our experimental conditions. The transitions accessed in the LIF detection scheme (Sec. II F) probed only the $\Pi(A')$ state.[18,19]

An advantage of the use of photolysis rather than chemical reaction for generating rotationally excited OH is the separation of time scales between OH production and RET: generation of OH occurred only during the laser pulse, allowing subsequent rotational relaxation to be monitored without the complication of continued OH production.

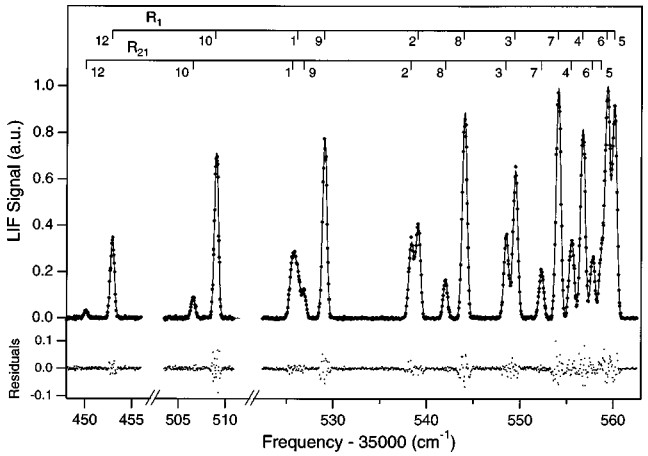

FIG. 1. OH $A\ ^2\Sigma^+(v'=1)-X\ ^2\Pi_{3/2}(v''=0)$ LIF spectrum (points) and the least-squares fit (line); the residuals are shown below the spectrum. Each point represents an average of 20 laser shots, corrected for the photolysis and probe powers on a shot-by-shot basis. Line assignments are given above the spectrum. The bath gas was Ar, the pressure was 7.7 Torr, and the delay between the photolysis and probe laser pulses was 10 ns. Note the scale discontinuities on the abscissa.

F. Determination of OH($v''=0,N''$) populations from the LIF spectra

The probe laser was tuned over the R_1 and R_{21} branches of the $A\ ^2\Sigma^+(v'=1)-X\ ^2\Pi_{3/2}(v''=0)$ transition with $N''=1-12$. For these branches, the total angular momentum (J'') is $N''+1/2$ and N' is equal to $N''+1$; both branches originate in the $\Pi(A')$ (or e) Λ doublet.[18,19] $N''=11$ was not recorded because of a spectral overlap with the $R_2(9)$ line.

Nonlinear least-squares fits to the LIF spectra were used to extract relative populations of the OH($v''=0,N''$) levels. Line positions were taken from Dieke and Crosswhite,[19] and B coefficients were calculated using the line strengths given in LIFBASE.[20] Each spectrum was modeled as a sum of Gaussian profiles whose widths were varied in the fitting procedure to account for variations in the laser linewidth and in the OH Doppler width following photolysis (important only at the earliest times). The line positions were also allowed to vary (slightly) to account for nonlinearities in the scanning rate of the DFDL. The integrated line intensity of each N'' level was determined from a weighted average of the integrated line intensities for the corresponding main (R_1) and satellite (R_{21}) branches. A representative OH LIF spectrum and the corresponding fit are shown in Fig. 1; Fig. 2 shows spectra at various pressure-time products for two bath gases.

To obtain relative populations, the integrated line intensities from the spectral fits were corrected for variations in the fluorescence quantum yield (Φ) with N' according to

$$\Phi=\frac{A}{A+k_B[B]+k_{H_2O}[H_2O]}, \tag{1}$$

where A is the spontaneous emission rate, k_X is the OH collisional quenching rate for molecule X, $[X]$ is the density of

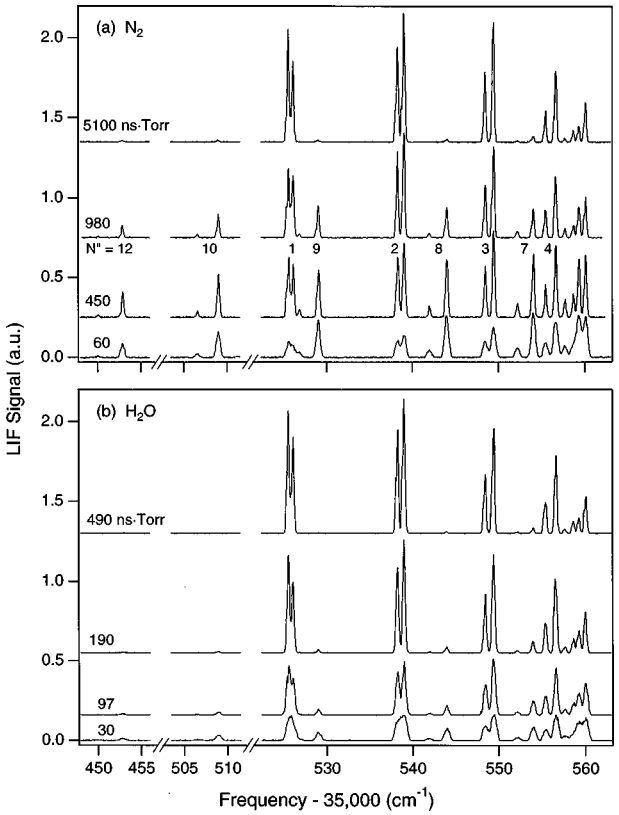

FIG. 2. OH($v''=0$) LIF spectra at the indicated pressure-time products following 266-nm photolysis of H_2O_2 for the bath gases (a) N_2 (6.3 Torr) and (b) H_2O (0.98 Torr). Note the scale discontinuities on the abscissa.

X, and B denotes the bath gas. Both A and k_X are functions of N'. A values were obtained from LIFBASE.[20] k_X values were determined from Gaussian fits to literature values[21–25] of k_X vs N' (these fits were required to interpolate and extrapolate the reported quenching rates to unmeasured N'). For the range of conditions in the present experiment, Φ varied between 0.015 and 0.54, the variation with bath gas was more pronounced than that with N' (less than $\pm 27\%$ variation for a given bath gas).

At early times, the spectral lines were broadened due to the large translational energy imparted to the OH fragments by the photodissociation [e.g., the bottom spectra in Figs. 2(a) and 2(b)]. Because OH translational relaxation is faster than rotational relaxation for Ar, N_2, and O_2, the spectral lines sharpened prior to substantial cooling of the nascent rotational distribution for these bath gases; for H_2O, some RET had occurred before translational equilibration was complete (Sec. II E).

G. Experimental checks

A number of experimental checks were performed:

(1) As discussed in Sec. II C the composition of the aqueous H_2O_2 solution was checked by measuring its density and UV absorption spectrum.
(2) In most of the experiments, OH rotational distributions were measured at a fixed pressure with various time delays between the photolysis and probe lasers. For the bath gases N_2 and H_2O, rotational distributions were recorded at a second pressure. The measured distributions at different pressures but the same pressure-time product were identical within experimental uncertainty, verifying that the results are independent of the residence time in the flow cell.
(3) The polarization of the probe laser was rotated by 90° (perpendicular photolysis and probe) to check for alignment or orientation effects; no difference in the measured OH rotational distributions was observed.
(4) The photolysis and probe power dependences were recorded several times throughout the course of these experiments to ensure that the LIF signal was linear in both the photolysis and probe powers, i.e., that neither the photolysis nor the LIF transitions were saturated.

III. RESULTS

A. Measured OH rotational distributions

Figure 2(a) shows OH LIF spectra recorded at various times following H_2O_2 photolysis in N_2; Fig. 2(b) shows a similar set of spectra, but with H_2O as the bath gas. The dramatically faster RET rate of H_2O is evident from these figures; for example, the OH rotational distribution is nearly thermal by 190 ns·Torr for H_2O, while significant population is observed in $N''=7-12$ at 980 ns·Torr for N_2.

The time evolution of the OH($v''=0$) rotational distribution is most conveniently presented as a Boltzmann plot [i.e., a plot of the population of each N'' level divided by the level degeneracy $(2N''+2)$ versus the rotational energy] at various pressure-time products. Such plots are shown in Figs. 3–6 for the bath gases Ar, N_2, O_2, and H_2O, respectively. The OH rotational distributions for Ar, N_2 and O_2 have qualitatively similar behavior: the lowest rotational levels ($N''<6$) attain thermal equilibrium relatively quickly, while the higher levels relax on a slower time scale, resulting in a kinked rotational distribution at intermediate times. OH in H_2O behaves differently, however: in addition to having an overall faster relaxation rate, the difference in relaxation rates between high and low N'' is not as pronounced, leading to only slight curvature of the Boltzmann plot; the rotational relaxation is primarily characterized by a monotonic increase in the slope with time. These observations will be made more quantitative in Sec. IV A, in which modeling of the OH rotational relaxation is discussed.

For Ar, N_2, and O_2, the initial OH rotational distribution is well characterized by a temperature of 1660 ± 120 K, in good agreement with previous experiments (1530 ± 150 K).[17] Moreover, the OH linewidths had narrowed to their room-temperature values by ~200 ns·Torr, before significant rotational relaxation had occurred. This result confirms that translational relaxation of the nascent OH occurs on a time scale faster than RET for these bath gases. For H_2O, some rotational relaxation had occurred at the earliest time, as seen in Fig. 6 (and as mentioned in Sec. II E).

The measured rotational distributions have a small contribution from OH produced by H_2O_2 photolysis by the probe laser. This contribution, which was most significant for high N'' at late times, was measured to be generally $<1\%$ and always $<3\%$. Because this interference was minor, no cor-

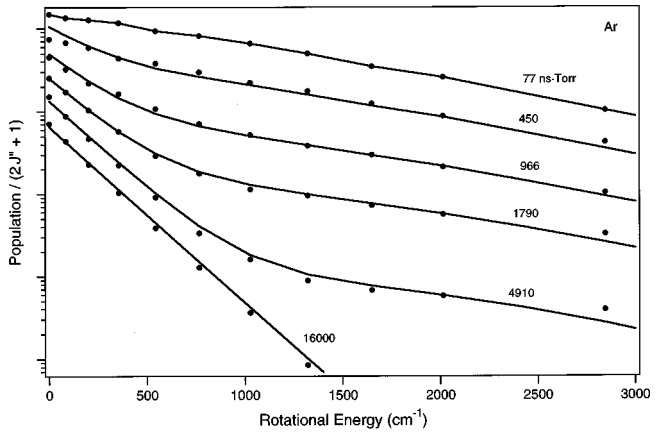

FIG. 3. Boltzmann plots of the OH($v''=0$) rotational distribution at the indicated pressure-time products following 266-nm photolysis of H_2O_2 in Ar at 7.9 Torr. The points are the experimental data; the lines are the corresponding distributions from the best-fit exponential-gap model (Model 1, Sec. III B). Data at the different times have been offset for clarity.

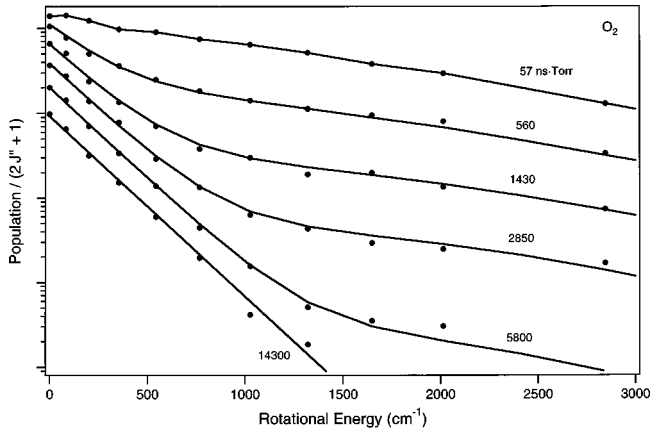

FIG. 5. Same as Fig. 3, but for O_2 bath gas at 2.8 Torr.

rection was applied to the data. Similarly, the small amount (<1%) of H_2O present in the Ar, N_2, and O_2 (from the aqueous H_2O_2 solution) contributed to the measured RET rates for these bath gases. Quantification of the H_2O contribution requires knowledge of the form of the RET rate matrix (see below) and is discussed in Sec. IV A.

B. RET models

The present measurements do not provide a unique determination of the matrix of state-to-state RET rate constants, **k**. The elements of **k** are denoted k_{fi}, where f and i correspond to the final and initial rotational states (N_f and N_i, respectively). By assuming a functional form for the dependence of k_{fi} on N_f and N_i, however, **k** can be determined from a fit to the measured rotational population distributions. We investigated several functional forms for **k**, including,

(1) exponential gap: $k_{fi}=\alpha\ \exp\{-\beta(E_f-E_i)/k_BT\}$,

(2a) modified exponential gap:
$k_{fi}=\alpha(1+\gamma N_i)\exp\{-\beta(E_f-E_i)/k_BT\}$,

(2b) modified exponential gap:
$k_{fi}=\alpha\ \exp\{-\beta(1+\gamma N_i)(E_f-E_i)/k_BT\}$,

(3) m_J-scrambling exponential gap:
$k_{fi}=\alpha(2N_f+2)\exp\{-\beta(E_f-E_i)/k_BT\}$, and

(4) $\Delta N''=\pm 1$: $k_{fi}=\alpha_i\delta(N_f,N_i+1)$.

In these formulas, α, β, and γ are adjustable parameters, E_f and E_i denote the rotational energies of levels N_f and N_i, respectively, k_B is Boltzmann's constant, and T is the absolute temperature (293 K for the present experiment); k_{fi} represents an upward rate ($N_f>N_i$), and the downward rates were determined by microscopic reversibility.

Model 1 is the standard exponential-gap form, which has often been found to provide a good description of RET rates.[26,27] The modified exponential-gap formulas, 2a and 2b, allow a first-order dependence of α or β on N_i. Model 3 weights k_{fi} by the degeneracy of the final state, $(2N_f+2)$. Model 4 allows transitions only between adjacent rotational levels (α_i may be different for each N_i); this model was used by Holtzclaw *et al.*[8] to fit their OH RET data.

The best-fit parameters for each model and bath gas were determined by minimizing the function

$$\chi=\sum_{j=1}^{T_f}\sum_{N''=1}^{12}\left(\frac{P_{\mathrm{meas}}(t_j;N'')-P_{\mathrm{calc}}(t_j,N'')}{P_{\mathrm{meas}}(t_j,N'')}\right)^2, \qquad (2)$$

where j, the time index, runs from 1 (the initial time) to T_f (the final time), $P_{\mathrm{meas}}(t_j,N'')$ is the measured population of

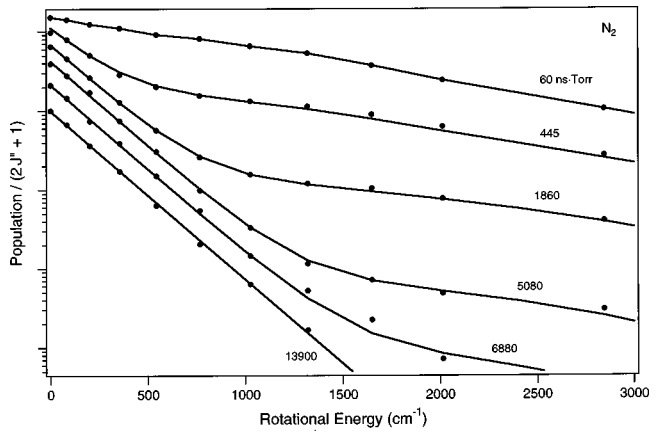

FIG. 4. Same as Fig. 3, but for N_2 bath gas at 6.2 Torr.

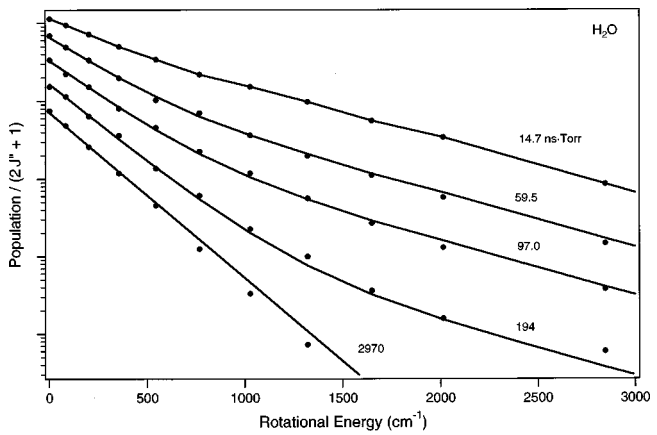

FIG. 6. Same as Fig. 3, but for H_2O bath gas at 0.98 Torr.

TABLE I. Best-fit parameters[a] for the exponential-gap and modified exponential-gap RET models.

Bath gas	Model	α	β	γ
Ar	1	1.0	1.73	⋯
	2a	0.44	1.34	−0.062
	2b	0.38	1.28	0.019
N_2	1	4.0	2.06	⋯
O_2	1	1.3	1.67	⋯
	2a	0.82	1.42	−0.041
	2b	0.73	1.40	0.0093
H_2O	1	4.2	1.21	⋯

[a]Units of α are 10^{-10} cm^3 s^{-1}; β and γ are unitless.

level N'' at time t_j, and $P_{\mathrm{calc}}(t_j,N'')$ is the corresponding calculated population. The calculated populations were determined by evaluating the expression

$$\mathbf{P}_{\mathrm{calc}}(t_j)=\exp\{\mathbf{k}(t_j-t_1)\}\mathbf{P}_{\mathrm{meas}}(t_1), \tag{3}$$

where $\mathbf{P}_{\mathrm{calc}}(t_j)$ is the vector of populations, $\{P_{\mathrm{calc}}(t_j,N'')\}$, at time t_j, and $\mathbf{P}_{\mathrm{meas}}(t_j)$ is the corresponding measured population vector. Note that the calculation was initialized with the rotational distribution measured at t_1 (i.e., at the smallest pressure-time product). In evaluating χ, we omitted levels that were not measured because their populations were too small (high N'' at large t) or because of spectral interference ($N''=11$). Minimization of χ was performed using the software STEPIT.[28]

To ensure conservation of population in the measured rotational distributions, the (unmeasured) populations of $N''=11$, 13, and 14 were filled in by interpolating/extrapolating the measured populations of $N''=10$ and 12: the ''temperature'' corresponding to the $P_{\mathrm{meas}}(t_j,10)/P_{\mathrm{meas}}(t_j,12)$ ratio was determined for each j, and the corresponding populations of $N''=11$, 13, and 14 at this temperature were then calculated. This procedure ensured proper normalization of the measured population distributions (for comparison with the calculated distributions) and did not significantly influence the analysis. The populations of the interpolated and extrapolated levels were not included in the determination of χ.

The best-fit parameters for the exponential-gap model for the four bath gases are listed in Table I; the corresponding calculated rotational distributions are shown by the solid lines in Figs. 3–6. For Ar and O_2, the best-fit parameters for Models 2a and 2b are also given in Table I. These RET models are discussed further in the following section. We estimate the uncertainty of the model parameters to be approximately ±15% for α, ±5% for β, and ±5% for γ; these uncertainties are based on the results of multiple fits to each data set (i.e., they reflect the nonindependence of the parameters) and on fits to comparable data sets recorded on different days.

IV. DISCUSSION

A. RET models

As seen in Figs. 3–6, the exponential-gap model (Model 1) provides a remarkably good description of the observed time evolution of the OH rotational population distributions: this model is able to reproduce the kinked rotational distributions at intermediate times for Ar, N_2, and O_2 as well as the less-pronounced curvature of the Boltzmann plots for H_2O. These fits were obtained with only two adjustable parameters (α and β) for each bath gas.

By allowing a first-order dependence of α or β on N'' (Models 2a and 2b), a somewhat better fit was obtained for the bath gases Ar and O_2 (χ was decreased by 35% and 15%, respectively, compared to Model 1); this improvement was comparable for Models 2a and 2b, i.e., the data do not allow us to distinguish between these two models. For interpolation or extrapolation of the measured distributions, we recommend using the parameters from Model 2a or 2b for Ar and O_2. The modified exponential-gap models did not provide a significantly better fit for N_2 or H_2O.

The m_J-scrambling exponential-gap model (Model 3) was not as successful in fitting the observed distributions as the standard exponential-gap model for all bath gases: the values of χ were 4%–20% larger for Model 3 than for Model 1. Similarly, Chandler and Farrow[29] found close agreement with an exponential-gap model but unsatisfactory agreement with an m_J-scrambling exponential-gap model for their measured RET rates for HD($v''=1$) colliding with thermal HD at 296 K. Sitz and Farrow[30,31] measured state-to-state RET and alignment-transfer rates for $N_2(v''=1)$ in collisions with thermal N_2; this work showed directly that the rate of m_J-changing collisions is slower than that of J-changing collisions and that alignment (i.e., a nonstatistical m_J-state distribution) is preserved in J-changing collisions. Although the present OH RET results are consistent with this observation, they do not allow an explicit determination of the effect of collisions on the m_J-state distribution.

Model 4 ($\Delta N''=\pm1$) provided a better fit to the data than Model 1 (χ was reduced by 20%–40%). This result was expected because Model 4 has 12 adjustable parameters (one for each N'') while Model 1 has two parameters. Given this large increase in the number of adjustable parameters, the reduction in χ for Model 4 is minimal. Previous RET measurements[2,29,30,32] for both polar and nonpolar diatomic molecules have shown that $\Delta N''$ is not restricted to ±1, particularly at low N'', where the energy gaps are small ($B_e=18.9$ cm^{-1} for OH).[33] The exponential-gap results (Table I) indicate the importance of multiple-quantum transitions: k_{fi} is reduced by a factor of two from its maximum value when E_f-E_i is 67–120 cm^{-1} (depending on bath gas). We therefore conclude that Model 4 is unlikely to provide an accurate representation of the state-to-state RET rate matrix.

We used the calculated rate matrices to investigate the contribution of RET by H_2O to the other bath gases (Sec. III A). Specifically, subtracting $\mathbf{k}$ for H_2O (weighted by its mole fraction) from $\mathbf{k}$ derived for another bath gas measured in the presence of water yields $\mathbf{k}$ for the bath gas alone. For Ar (the bath gas with the slowest RET rate), removing the H_2O contribution to the exponential-gap rate matrix reduces α by 3.7% and β by 1.7%; for the N_2 and O_2, the effect is even smaller. We therefore conclude that the effect of the residual H_2O in the other bath gases is insignificant.

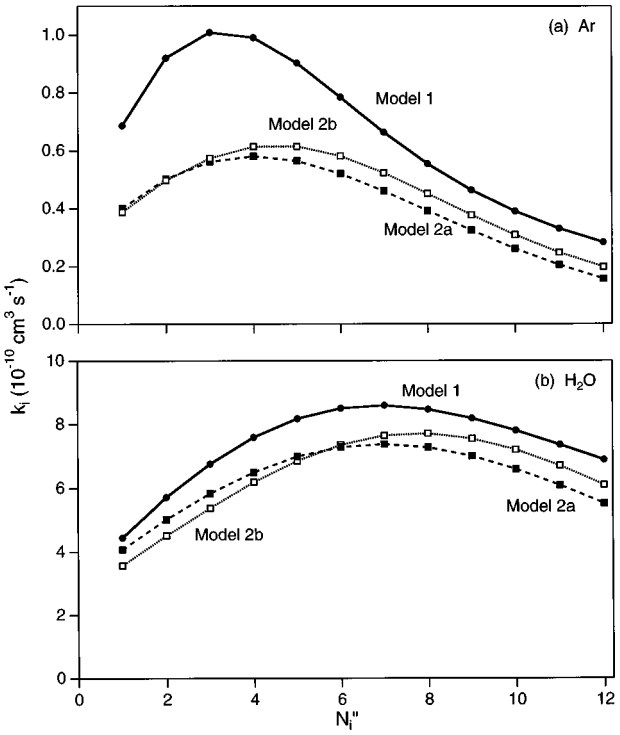

FIG. 7. Total depopulation rates, k_i (diagonal elements of **k**), calculated using the indicated RET models for (a) Ar and (b) H_2O.

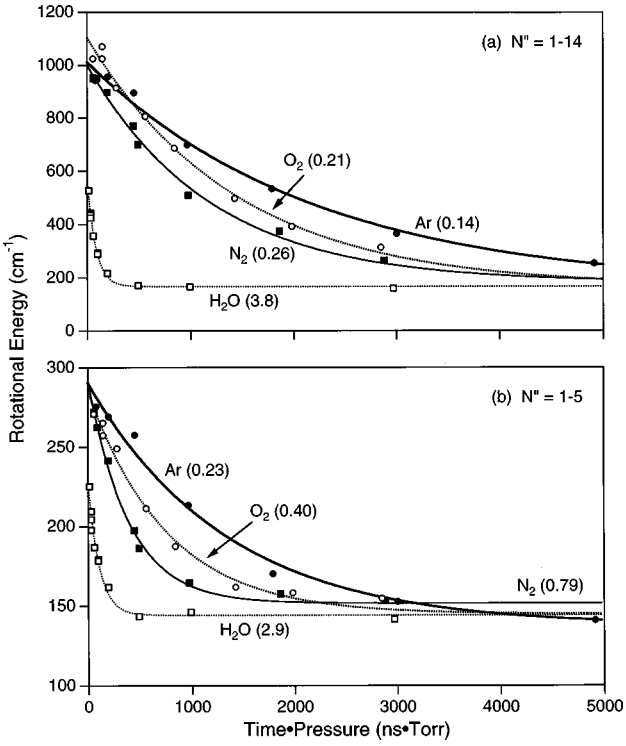

FIG. 8. Ensemble average of the OH($v''=0$) rotational energy versus pressure-time product for Ar, N_2, O_2, and H_2O: (a) $N''=1-14$, (b) $N''=1-5$. The points are the data, and the lines are single-exponential fits corresponding to the average RET ''rate constants'' shown in parentheses (units of 10^{-10} cm^3 s^{-1}). The ensemble-average rotational energy at time t_j is given by $\Sigma P_{meas}(t_j,N'')E_{N''}/\Sigma P_{meas}(t_j,N'')$, where the summations run over the relevant range of N''.

B. Total depopulation rates

For spectroscopic applications (e.g., determination of linewidths),[30] a particularly important parameter is the rate of population transfer out of a given level, *i*. These depopulation rates, denoted k_i, correspond to the diagonal matrix elements of **k**, i.e., $k_i=\Sigma_f k_{fi}$, where $f\neq i$ but f can be greater or less than i. Although the values of k_i are somewhat dependent on the assumed form of the rate matrix, they are better determined in the present experiment than are the individual state-to-state rate constants, k_{fi}.

Figure 7 shows the total depopulation rate as a function of N'' for the bath gases Ar and H_2O. The results of the exponential-gap and modified exponential-gap models are shown to indicate the model dependence of k_i. For Ar at low N'', Models 2a and 2b yield k_i values as much as 50% smaller than Model 1; this difference is generally diminished at higher N'', where k_i is dominated by downward, single-quantum transitions (i.e., where the energy gaps are large). For H_2O, the differences between the models are smaller ($\sim$15%), as expected from the χ values (Sec. IV A). We conclude that the present experiment is likely able to determine k_i values to an accuracy of $\sim\pm$50%. Plots of k_i vs N'' for N_2 and O_2 (not shown) are similar to that for Ar [Fig. 7(a)] in both shape and magnitude. In contrast, for H_2O [Fig. 7(b)], the k_i values are approximately an order of magnitude larger and depend less strongly on N'', consistent with stronger attractive forces for this bath gas.[21] Note that the differences between H_2O and the other bath gases are significantly larger than the uncertainties in k_i.

The results shown in Fig. 7 are in accord with the qualitative RET observations presented in Sec. III A concerning the dependence of the RET rate on N'' (i.e., the kinked rotational distributions for Ar, N_2, and O_2) and the differences between H_2O and the other bath gases.

C. Average relaxation rates

RET has often been characterized by a single ''rate'';[34] such an approach was taken by Gericke and Comes[7] to describe their measurements of OH($v''=0$) RET in collisions with H_2O. We have extracted ''average RET rate constants'' from our measured OH rotational distributions by calculating the ensemble average of the OH($v''=0$) rotational energy as a function of time (Fig. 8). To illustrate the N''-dependence of this rotational-relaxation ''rate,'' we compared the effect of including all of the levels in calculating the rotational energy [Fig. 8(a)] with including only the lowest five levels [Fig. 8(b)]. In all cases, the data are reasonably well described by single exponential decays, from which the average RET rate constants given in Fig. 8 are obtained. The rate constants for Ar, N_2, and O_2 are a factor of $\sim$2 smaller for $N''=1-5$ than for $N''=1-14$. In contrast, the average RET rate constant for H_2O is not strongly dependent on the number of levels included in the analysis.

D. Comparison with previous results

We can compare our results with several previous RET studies of both ground-state and electronically excited OH.

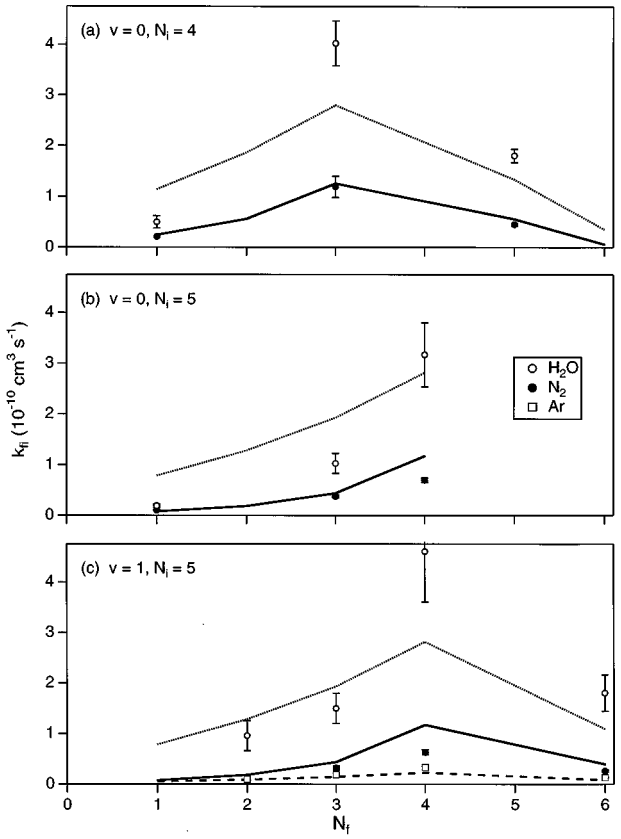

FIG. 9. Comparison of measured state-to-state RET rate constants (symbols, *A* state) (Refs. 35 and 36) with those derived from modeling of the present data (lines, *X* state) for the indicated bath gases. Noted in each panel are the initial rotational state (N_i) and the vibrational level of the state-to-state measurements (v); the abscissa corresponds to the final rotational state (N_f). For Ar, the lines correspond to Model 2b (which best reproduced the experimental results); for N_2 and H_2O, the lines correspond to Model 1 (which gave results indistinguishable from Model 2b). The *A*-state data refer to symmetry-preserving transitions within the F_2 manifold.

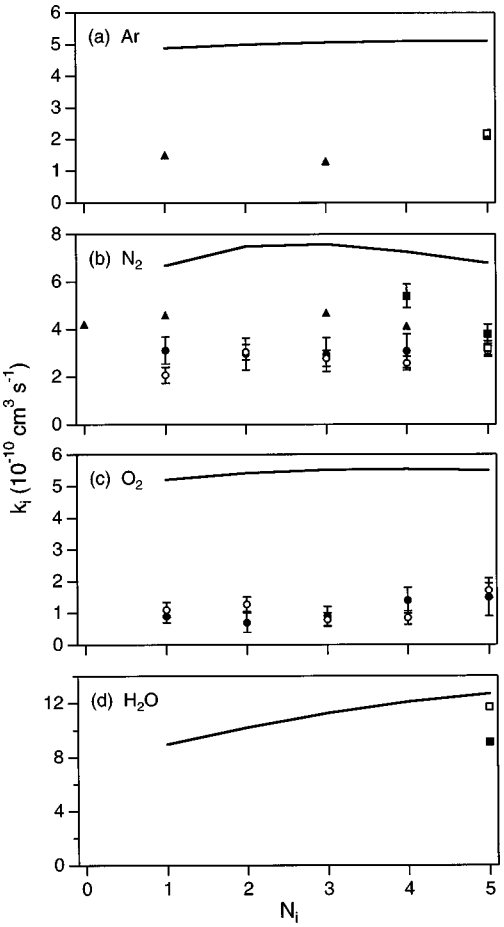

FIG. 10. Comparison of measured depopulation rate constants for the *A* state (symbols) with the present, *X*-state values (lines). Filled symbols denote $v'=0$ and open symbols denote $v'=1$; triangles are from Ref. 39, squares are from Ref. 36, filled circles are from Ref. 38, and open circles are from Ref. 23. The values from the present experiment include a correction for the contribution of nearly elastic, Λ-doublet-changing collisions (4.5×10^{-10} cm^3 s^{-1}).

1. State-to-state rate constants

We first compare the OH($X\ ^2\Pi_{3/2}, v''=0$) k_{fi} values derived from the present experiment with measured OH($A\ ^2\Sigma^+, v'=0,1$) state-to-state rate constants[35,36] (Fig. 9). Although there is no *a priori* reason to expect comparable RET rates in the *X* and *A* states, Zizak *et al.*[37] found them to be similar; specifically, by modeling saturated OH LIF measurements, they concluded that RET is 30% faster in the *X* state than in the *A* state. Similarly, comparison of the present $v''=0$ measurements with *A*-state data for both $v'=0$ and $v'=1$ is justified because the RET rates in these two vibrational levels are nearly equal.[23,35,36,38] As shown in Fig. 9, the agreement between the previously measured and our derived k_{fi} values is surprisingly good, both for the magnitude of the rate constants and for their dependence on ΔN and bath gas. The main area of disagreement is for H_2O, which shows a stronger dependence on ΔN (i.e., a stronger preference for $\Delta N=-1$) in the state-to-state measurements. We cannot determine if this result reflects a real difference between the *X* and *A* states or is an artifact of the RET model used to analyze the present data.

2. Depopulation rate constants

Depopulation rate constants, k_i, have been reported for both the *A* and *X* states. Care must be taken in comparing our k_i values (the diagonal matrix elements) with other measurements because we detected only one of the Λ doublets (Sec. II F). Previous studies have shown that nearly elastic, Λ-doublet-changing collisions ($\Delta N''=0, \Delta J''=0$) are rapid: for OH($X\ ^2\Pi_{3/2}, v''=2, J''=1.5$) colliding with H_2O, the rate constant for such $e\leftrightarrow f$ transfer is 4×10^{-10} cm^3 s^{-1} (Ref. 10); for OH($X\ ^2\Pi_{3/2}, v''=1, J''=1.5$) colliding with H_2, the rate constant is $(5.1\pm1.1)\times10^{-10}$ cm^3 s^{-1} (Ref. 9). For comparison with previous measurements, we therefore added 4.5×10^{-10} cm^3 s^{-1} (the average of the two $e\leftrightarrow f$ rate-constant measurements) to the k_i values derived from the RET models; this procedure is reasonable because (i) the $e\leftrightarrow f$ rate does not appear to have a strong dependence on v'' or bath gas, and (ii) for the range of N'' under consideration, the Λ-doublet splitting is <2 cm^{-1}, i.e., we do not anticipate a strong dependence of the rate on N''.

Copeland and Crosley[10] measured k_i to be 9×10^{-10} cm^3 s^{-1} for OH($X\ ^2\Pi_{3/2}, v''=2, J''=1.5$) colliding with H_2O, in excellent agreement with the present value of

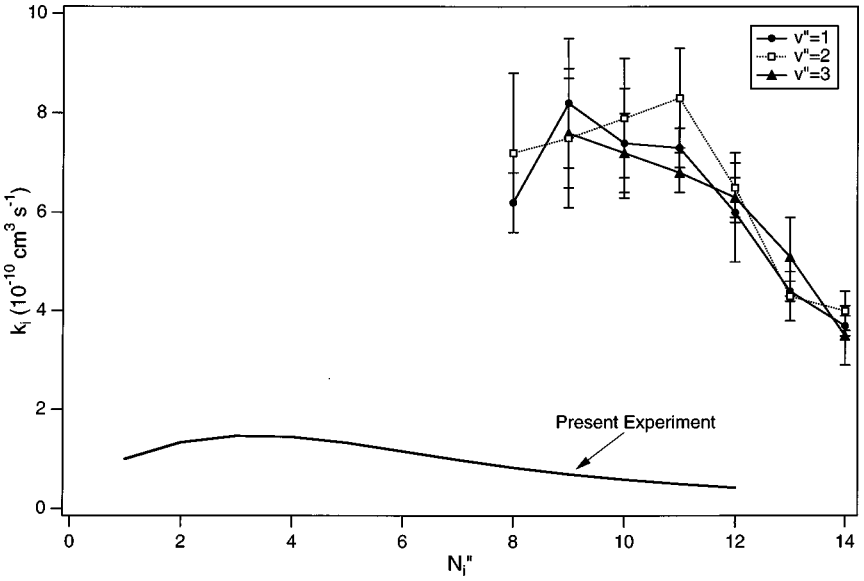

FIG. 11. Comparison of the OH depopulation rate constants derived from the present experiment (293 K, $v''=0$) to those of Holtzclaw *et al.* (Ref. 8) (100 K, $v''=1-3$) for collisions with O_2.

8.9×10^{-10} cm^3 s^{-1} for OH($v''=0,J''=1.5$). Andresen *et al.*[9] obtained a similar value of $(5-9)\times10^{-10}$ cm^3 s^{-1} for collisions of OH($v''=1,J''=4.5$) with H_2O_2.

Figure 10 shows a comparison of previously measured depopulation rate constants for the *A* state[23,36,38,39] with our calculated, *X*-state values for all four bath gases. The *A*-state rates are generally larger than the present rates, in accord with the conclusion of Zizak *et al.*[37] For Ar, N_2, and O_2, the *X*-state rates are larger by factors of $\sim2-7$; this difference is almost wholly accounted for by the contribution of $e\leftrightarrow f$ exchange to k_i, i.e., rotationally inelastic energy-transfer rates are nearly equal in the two electronic states (as indicated in Fig. 9). For H_2O, the $e\leftrightarrow f$ rate constant is a smaller fraction of k_i, and the *X*-state and *A*-state depopulation rate constants are therefore nearly equal. For Ar, N_2, and O_2, k_i is not strongly dependent on N_i in either the *A* or *X* state for the range $N_i=1-6$.

Holtzclaw *et al.*[8] reported RET rate constants for the process OH(v'',N'')+$O_2\rightarrow$OH($v'',N''-1$)+O_2 for $v''=1-3$ at 100 K. Because the data analysis assumed no multiple-quantum transitions (Model 4, $\Delta N''=\pm1$), these rate constants correspond to depopulation rates, k_i (for the range of N'' under consideration, the correction for transitions with $\Delta N''=+1$ is insignificant). Moreover, these rate constants are directly comparable to our depopulation rate constants because both experiments were characterized by an equilibrium distribution between the Λ-doublet levels. Our results are compared to those of Holtzclaw *et al.* in Fig. 11. Where the data sets overlap ($N''=8-12$), our k_i values are a factor of ~10 smaller than the previous values. This discrepancy is puzzling. It is likely partially attributable to the assumption of $\Delta N''=\pm1$ in the data analysis procedure of Holtzclaw *et al.*: Model 4 yields consistently larger k_i values than any of the other models (although it is able to fit both our data set and that of Holtzclaw *et al.*); this result, however, accounts for no more than a factor of two for $N''=8-12$. The main differences between the two experiments were (i) we detected $v''=0$ while Holtzclaw *et al.* detected $v''=1-3$, and (ii) our experiment was performed at 293 K while that of Holtzclaw *et al.* was performed at 100 K. The former difference is unlikely to account for a factor of 5–10 because the RET rates are not strongly dependent on v''.[8,23,36,38] Although a rapid increase in the RET rate with decreasing temperature could account for the discrepancy, OH pressure-broadening measurements[40,41] indicate that this increase would have to occur at temperatures below 200 K (see below).

3. Pressure-broadening coefficients

The width of absorption lines is often determined by collisional processes. If elastic dephasing collisions are assumed to make an insignificant contribution to the linewidth, the pressure-broadening coefficient for the transition between levels N_i and N_f(γ_{if}, FWHM) is related to the total depopulation rates of these levels ($k_i^{\rm tot}$ and $k_f^{\rm tot}$, respectively) by:[42]

$$\gamma_{if}=\frac{k_i^{\rm tot}+k_f^{\rm tot}}{2\pi c}, \tag{4}$$

where $k_i^{\rm tot}$ and $k_f^{\rm tot}$ include RET and, where relevant, vibrational energy transfer and electronic quenching.

Table II compares measured pressure-broadening coefficients of several OH lines with values calculated using Eq. (4). The first five entries refer to microwave transitions within $v''=0$ of the $X\ ^2\Pi_{3/2}$ state, and the remaining entries refer to the $P_1(2)$UV$A(v'=0)-X(v''=0)$ transition. For the *X* state, only RET contributes to the depopulation rates ($k_j^{\rm tot}=k_j$), and we used the k_j values obtained from the present experiment (e.g., Fig. 10). For the *A* state, we used measured depopulation rates ($k_f^{\rm tot}$ including RET and quenching) for N_2 and O_2[38]; for Ar, we used the k_f value (RET only) for $F_2(5)$ in $v'=1$ of Kienle *et al.*[36] (this approximation is justified because electronic quenching by Ar is insignificant and γ_{if} for this transition is dominated by RET in the ground state). Note that for $A-X$ transitions with $v'>0$, vibrational energy transfer will contribute to $k_f^{\rm tot}$.[25]

TABLE II. Calculated and measured OH pressure-broadening coefficients (γ_{if}, FWHM) at ~300 K.

Transition[a]	Bath gas	Calculated coefficient[b] (cm^{-1} atm^{-1})	Measured coefficient (cm^{-1} atm^{-1})	Ref.
$X;\ J''=1.5\rightarrow J''=2.5$	Ar	0.13	0.0999 ± 0.0004	43
	N_2	0.19	0.194 ± 0.003	41
	O_2	0.14	0.134 ± 0.004	41
$X;\ J''=2.5\rightarrow J''=3.5$	N_2	0.20	0.182 ± 0.003	40
	O_2	0.15	0.096 ± 0.012	40
$X,\ J''=2.5\rightarrow A,\ J'=1.5$	Ar	0.094	0.141 ± 0.002	44
	N_2	0.20	0.217 ± 0.005	44
	O_2	0.10	0.143 ± 0.005	44

[a]X denotes the $^2\Pi_{3/2}(v''=0)$ state; A denotes the $^2\Sigma^+(v'=0)$ state.
[b]Using Eq. (4).

The agreement between the measured and calculated γ_{if} values is remarkably good. In particular, Eq. (4) correctly predicts the dependence of the linewidth on bath gas for both the microwave and the UV transitions ($Ar \leqslant O_2 < N_2$). The calculated pressure-broadening coefficients for the $A-X$ transition are ~30% too small for O_2 and Ar, presumably because of the neglect of collisional dephasing; a calculation of γ_{if} that includes only RET in the X and A states shows that RET accounts for over half of the pressure broadening for this transition for all three bath gases. These results indicate that RET dominates pressure broadening for the OH microwave transitions and makes a significant contribution to broadening of the UV transitions. Note that nearly elastic, Λ-doublet-changing collisions are the dominant contributor to the X-state depopulation rates, and hence to the pressure-broadening coefficients, for Ar, N_2, and O_2; however, the calculated dependence on bath gas derives from variations in the rate of rotationally inelastic collisions.

The microwave pressure-broadening measurements provide information on the temperature dependence of OH ground-state RET rates. Chance *et al.*[40] and Park *et al.*[41] measured a change of <30% in γ_{if} for O_2 upon decreasing the temperature from 296 to ~200 K. If the discrepancy discussed above between the present results and those of Holtzclaw *et al.*[8] is caused by an increase in the RET rate with decreasing temperature, this increase must therefore occur between 200 and 100 K.

4. Other comparisons

Gericke and Comes[17] reported an ''RET rate constant'' of $(2.2\pm0.5)\times10^{-10}$ $cm^3\ s^{-1}$ for OH($v''=0$) colliding with H_2O. This value is in reasonably good agreement with our ''average RET rate constant'' for H_2O of 3.8×10^{-10} $cm^3\ s^{-1}$ [Sec. IV C, Fig. 8(b)].

Holtzclaw *et al.* reported that OH RET by Ar is at least two orders of magnitude slower than RET by O_2.[8] Although our results also show Ar to be slower than O_2, we found this difference to be no more than a factor of two (e.g., Fig. 8). Similarly, Ar and O_2 have comparable depopulation rate constants for A-state OH [Figs. 10(a) and 10(c)].

V. CONCLUSIONS

From measurements of the collisional relaxation of a hot OH($^2\Pi_{3/2}, v''=0$) rotational distribution, we have derived OH($N''=1-12$) RET rate constants at 293 K for the bath gases Ar, N_2, O_2, and H_2O. These and previous measurements show that:

(1) RET rates for H_2O are approximately an order of magnitude faster than for the other bath gases;
(2) For Ar, N_2, and O_2, RET rates are significantly faster at low N'' than high N''; for H_2O, the RET rate is not as strongly dependent on N'';
(3) For Ar, N_2, and O_2, the total depopulation rate of a given level is dominated by nearly elastic, Λ-doublet-changing collisions ($\Delta N''=0, \Delta J''=0$); for H_2O, rotationally inelastic collisions ($\Delta N''\neq0$) are comparably important;
(4) RET is the dominant source of pressure broadening for OH microwave transitions;
(5) RET makes a significant contribution to pressure broadening for OH UV $A-X$ transitions;
(6) Rotationally inelastic energy-transfer rates are similar in the X and A states, but total RET rates (including Λ-doublet-changing collisions) are faster in the X state than the A state; and
(7) Multiple-quantum transitions make a significant contribution to OH rotational relaxation.

We find generally good agreement with previous OH RET and pressure-broadening measurements. One exception is the study of Holtzclaw *et al.*,[8] who obtained RET rate constants for collisions with O_2 at 100 K that are a factor of ~10 larger than the present values. This previous experiment predicts a microwave pressure-broadening coefficient at 100 K that is an order of magnitude larger than the measured values at 300 and 200 K.[40,41] Holtzclaw *et al.* reported that OH RET is a factor of >100 faster for O_2 than for Ar; the present study yielded a factor of <2.

The present data are well described by an exponential-gap model for the state-to-state RET rate matrix. This observation does not permit the conclusion that the actual rate matrix is characterized by an exponential-gap law. State-to-state measurements are required to gain a detailed understanding of OH RET, to resolve the remaining discrepancies, and to investigate more quantitatively the conclusions outlined above.

ACKNOWLEDGMENTS

This work was supported by the U.S. Department of Energy, Office of Basic Energy Sciences, Division of Chemical Sciences. We acknowledge the expert technical assistance of P. Schrader. We thank D. R. Crosley and G. E. Caledonia for helpful discussions.

[1] A. C. Eckbreth, *Laser Diagnostics for Combustion Species and Temperature* (Gordon and Breach, Amsterdam, 1996).
[2] K. Kohse-Höinghaus, Prog. Energy Combust. Sci. **20**, 203 (1994).
[3] A. Schiffman and D. W. Chandler, Int. Rev. Phys. Chem. **14**, 371 (1995).
[4] D. R. Crosley and G. P. Smith, Combust. Flame **44**, 27 (1982).
[5] R. Kienle, M. P. Lee, and K. Kohse-Höinghaus, Appl. Phys. B: Lasers Opt. **65**, 583 (1996).
[6] P. J. Dagdigian, in *Dynamics and Kinetics of Small Radicals*, edited by K.

Liu and A. F. Wagner (World Scientific, Singapore, 1995), p. 315.
[7] K.-H. Gericke and F. J. Comes, Chem. Phys. **65**, 113 (1982).
[8] K. W. Holtzclaw, B. L. Upschulte, G. E. Caledonia, J. F. Cronin, B. D. Green, S. J. Lipson, W. A. M. Blumberg, and J. A. Dodd, J. Geophys. Res. **102**, 4521 (1997).
[9] P. Andresen, N. Aristov, V. Beushausen, D. Häusler, and H. W. Lülf, J. Chem. Phys. **95**, 5763 (1991).
[10] R. A. Copeland and D. R. Crosley, J. Chem. Phys. **81**, 6400 (1984).
[11] I. J. Wysong, J. B. Jeffries, and D. R. Crosley, J. Chem. Phys. **94**, 7547 (1991).
[12] P. Andresen, D. Häusler, and H. W. Lülf, J. Chem. Phys. **81**, 571 (1984).
[13] D. M. Sonnenfroh, R. G. Macdonald, and K. Liu, J. Chem. Phys. **94**, 6508 (1991).
[14] K. Schreel, J. Schleipen, A. Eppink, and J. J. ter Meulen, J. Chem. Phys. **99**, 8713 (1993).
[15] W. C. Schumb, C. N. Satterfield, and R. L. Wentworth, Hydrogen Peroxide (American Chemical Society, Reinhold, New York, 1955).
[16] R. C. Taylor and P. C. Cross, J. Am. Chem. Soc. **71**, 2266 (1949).
[17] K.-H. Gericke, S. Klee, F. J. Comes, and R. N. Dixon, J. Chem. Phys. **85**, 4463 (1986).
[18] M. H. Alexander *et al.*, J. Chem. Phys. **89**, 1749 (1988); We use the following notation: v is the vibrational quantum number; N is the angular momentum quantum number excluding spin; J is the total angular momentum quantum number; single and double primes denote the excited and ground electronic states, respectively.
[19] G. H. Dieke and H. M. Crosswhite, J. Quant. Spectrosc. Radiat. Transf. **2**, 97 (1962).
[20] J. Luque and D. R. Crosley, SRI International, Report MP 96-001 (1996).
[21] R. A. Copeland, M. J. Dyer, and D. R. Crosley, J. Chem. Phys. **82**, 4022 (1985).
[22] R. A. Copeland, M. L. Wise, and D. R. Crosley, J. Phys. Chem. **92**, 5710 (1988).
[23] J. Burris, J. J. Butler, T. J. McGee, and W. S. Heaps, Chem. Phys. **124**, 251 (1988).
[24] C. B. Cleveland and J. R. Wiesenfeld, Chem. Phys. Lett. **144**, 479 (1988).
[25] L. R. Williams and D. R. Crosley, J. Chem. Phys. **104**, 6507 (1996).
[26] J. C. Polanyi and K. B. Woodall, J. Chem. Phys. **56**, 1563 (1972).
[27] D. F. Heller, Chem. Phys. Lett. **45**, 64 (1977).
[28] J. P. Chandler, Quantum Chemistry Program Exchange **11**, 307 (1976); available on the World Wide Web at www.osc.edu/cca/html_pages/qcpe.
[29] D. W. Chandler and R. L. Farrow, J. Chem. Phys. **85**, 810 (1986).
[30] G. O. Sitz and R. L. Farrow, J. Chem. Phys. **93**, 7883 (1990).
[31] G. O. Sitz and R. L. Farrow, J. Chem. Phys. **101**, 4682 (1994); **103**, 489E (1995).
[32] E. A. Rohlfing, D. W. Chandler, and D. H. Parker, J. Chem. Phys. **87**, 5229 (1987).
[33] K. P. Huber and G. Herzberg, *Constants of Diatomic Molecules* (Van Nostrand Reinhold, New York, 1979).
[34] J. D. Lambert, *Vibrational and Rotational Relaxation in Gases* (Oxford University Press, Oxford, 1977).
[35] A. Jörg, U. Meier, R. Kienle, and K. Kohse-Höinghaus, Appl. Phys. B: Photophys. Laser Chem. **55**, 305 (1992).
[36] R. Kienle, A. Jörg, and K. Kohse-Höinghaus, Appl. Phys. B: Photophys. Laser Chem. **56**, 249 (1993).
[37] G. Zizak, G. A. Petrucci, C. L. Stevenson, and J. D. Winefordner, Appl. Opt. **30**, 5270 (1991).
[38] J. Burris, J. Butler, T. McGee, and W. Heaps, Chem. Phys. **151**, 233 (1991).
[39] R. K. Lengel and D. R. Crosley, J. Chem. Phys. **67**, 2085 (1977).
[40] K. V. Chance, D. A. Jennings, K. M. Evenson, M. D. Vanek, I. G. Nolt, J. V. Radostitz, and K. Park, J. Mol. Spectrosc. **146**, 375 (1991).
[41] K. Park, L. R. Zink, K. M. Evenson, K. V. Chance, and I. G. Nolt, J. Quant. Spectrosc. Radiat. Transf. **55**, 285 (1996).
[42] A. Schenzle and R. G. Brewer, Phys. Rev. A **14**, 1756 (1976).
[43] J. P. Burrows, D. I. Cliff, P. B. Davies, G. W. Harris, B. A. Thrush, and J. P. T. Wilkinson, Chem. Phys. Lett. **65**, 197 (1979).
[44] B. Shirinzadeh, D. M. Bakalyar, and C. C. Wang, J. Chem. Phys. **82**, 2877 (1985).